Politecnico di Milano

Orbital Mechanics

Final Report A.Y. 2022/2023

The ESA Wanabees

Group ID: 2233

Team members

Person Code	Surname (s)	Name	Matriculation N.
10913819	Albiñana Burdiel	Carlos	221327
10913857	Fernández Diz	Jaime	219094
10850084	Gao	Luca	100985
10724126	Marzorati	Emanuele	225268

Contents

1. *Interplanetary Explorer Mission*

1.1 Mission Description

The following assignment deals with the optimal design of an interplanetary transfer orbit to a Near Earth Object (NEO), with departure from Earth and performing a powered gravity assist in a Solar System Planet. The objective is to describe the methodology followed for the total Δv cost minimization process and asses the results within a time window. The initial heliocentric orbit is considered to be that of Earth and the final heliocentric orbit must be equal to the arrival asteroid.

This case has the following parameters:

- **Departure Planet:** Earth • **Earliest Departure:** 30/10/2026
- **Fly-by Planet:** Saturn • **Latest Arrival:** 27/04/2061

- **NEO:** 2002VD17 Apollo Class (ID 51)

1.2 Mission Design

1.2.1 Hypothesis and Design Constraints

The design process of this mission is based on the **patched conics approximation**, whereby an N-body problem is divided into multiple two body solutions. In the case of this project, the **Sphere of Influence** (SOI) of Saturn from a heliocentric point of view is considered point-like and the fly-by manoeuvre is instantaneous. The transfer orbit from Earth to Saturn is then calculated as a Lambert Arc connecting the positions of these planets in their departure and fly-by dates, respectively. A second Lambert arc is calculated, connecting Saturn and the NEO in its arrival date. These heliocentric velocities are then used to compute the powered fly-by parameters. As a result, the total mission Δv is the sum of the three manoeuvres: Earth Orbit Departure, Powered Gravity Assist and Arrival at NEO Orbit. Furthermore, the optimum result will be the combination of close but sub-optimum solutions of each section.

Additionally, Saturn's rings have been neglected in the powered fly-by computation. The only constraint set is a closest approach of 1.3 x Saturn's Radius from its center (75702 km). This distance was chosen as this was the closest approach performed by the *Cassini-Huygens* spacecraft in 2004 [1].

1.2.2 Numerical Approach

There are three **Degrees of Freedom** (DoFs) that govern this mission: **Time of Departure**, **Time of Gravity Assist** and **Time of Arrival**. As such, a 3D discrete grid can be generated and solved for each case. It is more adjustable, however, to use the equivalent DoFs of **Time of Flight** (ToF) for the grid generation.

The Synodic Periods of Earth-Saturn (378 days), Saturn - NEO (721 days) and Earth-NEO (794 days) could be used to estimate a suitable time window of operation. Theoretically, a time step equal to the synodic period between Earth and NEO could be implemented. However, later tests showcased that the low cost regions repeat for a departure time that does not equate to the frequency of these periods. Therefore, the approach of constructing a coarse initial grid to locate the departure times with lower total mission Δv is selected. Out of all the possible cases, very few solutions will yield satisfactory results, leading to an unnecessarily high computational cost. An iterative process to reduce the time of computation and increase the grid precision is implemented. After a initial coarse grid search, the lowest total Δv is used as a cut-off condition to stop the computation of that specific branch. **I.e**, if the best Δv from the previous coarse grid was 18.5 km/s, there is no point in computing a whole branch where the departure cost is already higher than 18.5 km/s.

Once a low cost region is located, a similar approach is followed. The time of flight to both celestial objects from the best cases are selected and refined in this region, increasing the precision and lowering the amount of unnecessary computation. A pseudo-code explaining this procedure is seen below.

Moreover, given the nature of the mission, it is estimated that the optimum solution will occur when the Spacecraft's own perihelion intercepts the NEO at its perihelion or aphelion, where its relative velocities are lowest, as both orbits are going to be close to tangent.

Algorithm 1: 3 DoFs mission cost computation

```
foreach time of departure do
    pos_Earth ← Position of Earth at time_dep{i};
    foreach time of Flight to GA do
        time_GA ← time_dep + ToF_GA{j};                          /* GA == Gravity Assist */
        if time_GA>time of latest arrival then
            break ;                                              /* Go back to Departure Time */
        end
        Departure Δv ← Lambert{Position of Earth at time_dep{i}, Position of Saturn at timetime_GA{j}};
        if Departure Δv > Departure Δv cut-off then
            continue ;                                           /* Go back to ToF_GA */
        end
        foreach time of Flight to NEO do
            time_arr ← time_GA + ToF_arr{k};
            if time_arr>time of latest arrival then
                break ;                                          /* Go back to ToF_GA */
            end
            Arrival Δv ← Lambert{Position of Saturn at time_GA, Position of NEO at time_arr};
            if Arrival Δv > Arrival Δv cut-off then
                continue ;                                       /* Go back to ToF_arr */
            end
            Solve Powered fly-by parameters;
            if radius of perigee ≤ 1.3^ Radius of Saturn then
                continue ;                                       /* Go back to ToF_arr */
            end
            Total Δv = Departure Δv + Arrival Δv + GA Δv
        end
    end
end
```

1.3 Grid Search Results

1.3.1 Coarse Grid

An initial coarse grid is used to find suitable cut-off conditions for successive coarse grids. This way, the number of computed cases that satisfy all conditions and finish their computation is lowered from 16.2% down to 0.5%, even with a lower time step and finer mesh. This operation yields Figure 1.1, where the best 20000 cases are shown. Figure 1.1a shows that there are two distinct regions that yield low mission cost, corresponding to a longer and shorter time of transfer between the three celestial objects.

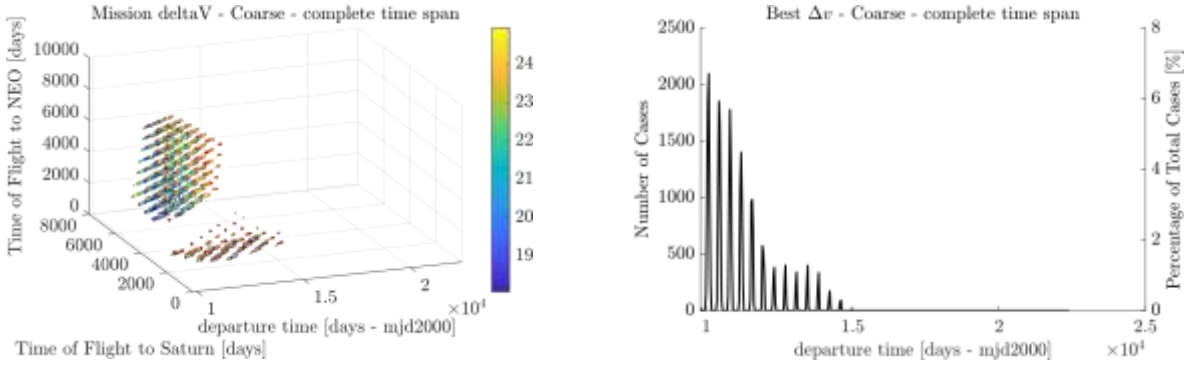

(a) Coarse Grid Visualization

(b) Low Δv cases per departure time

Figure 1.1: Coarse Grid Operation

This distinction is exemplified in Figure 1.3. Figure 1.1b shows that low mission cost is only associated, as expected, with certain departure dates with a periodicity of around 140 days and lasting between 280 days to just 90 days in later stages, as the only solution is that of shorter times of transfer. Also, no low cost solutions are found in the second half of the departure date DoF, corresponding to October 2043 onward. The reason for this is discussed at the end of Section 1.3.2.

It must be noted that these frequencies do not coincide with that of the Synodic Periods between the planets or the asteroid and hence why the successive coarse grid operations where done across the whole time span. As the proportion of computed cases is so low, a localized refinement is done on these departure dates that return lower Δv values.

1.3.2 Refined Grid

A localized refinement was performed on the time of departure windows seen in Figure 1.1b that showcased low mission cost. Figure 1.2 shows the grid visualization of the 5^{th} departure window, along with a comparison of the Time of Transfer of the 1000 best cases, which corresponds to the larger region seen besides.

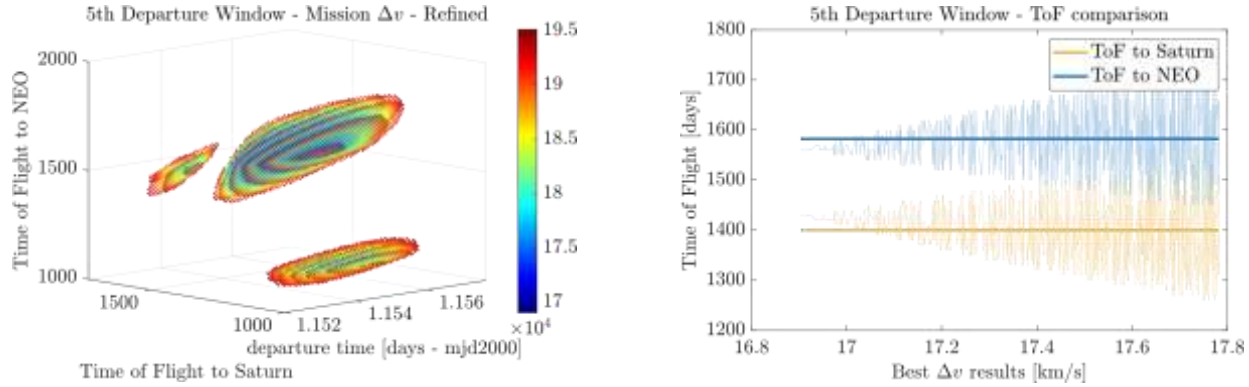

(a) Refined Grid Visualization

(b) Best Time of Flight Comparison

Figure 1.2: Refined Grid Search in 5^{th} departure window

This figure is chosen as it highlights the importance of performing a localized refinement due to the existence of smaller potentially desired regions that may go undetected under the coarse grid operation, leading to sub-optimal results. Following this refined study, the best departure time windows where selected for the final numerical optimization process.

Departure Window (#)	Best Δv [km/s]	Departure Time	ToF to GA [days]	ToF to NEO [days]
5	16.90	13/8/2031	1430	1560
1	17.34	31/7/2027	3410	3160
3	17.48	17/7/2029	1510	1520
6	17.56	30/8/2032	1270	1340
2	17.58	4/8/2028	3190	3020
4	17.61	31/7/2030	1330	1320

Table 1.1: Best Mission Cost Cases After Localized Refinement

Table 1.1 reveals what was seen in Figure 1.1, with two large distinct low cost regions characterized by short and long time of transfer. Figure 1.3 illustrates this phenomenon and sheds light as to why such distinct behaviours result is similar total mission cost.

The shorter time of flights correspond to an initial transfer arc to Saturn that reaches the celestial object once it has past its aphelion, whereas shorter time of flights have a Saturn transfer not exceeding this point of the orbit. All, however, coincide with the initial hypothesis discussed Section 1.2.1: Optimum transfer occurs when both the NEO and second transfer orbit's perihelion coincide. This is also the reason why the lower mission cost options are located in the first half of the total departure window, as this corresponds to Saturn being located opposite side to the NEO's aphelion in the heliocentric plane, allowing for this optimum configuration.

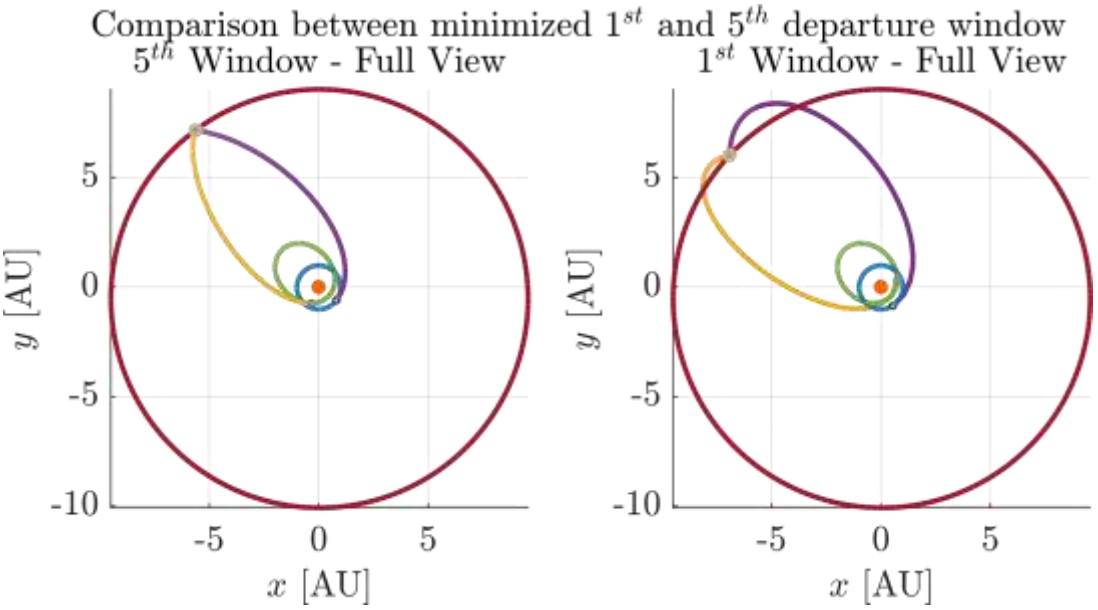

Figure 1.3: Comparison between the two best mission cost cases

1.4 Optimum Mission

In table 1.1, the runner-up options all exhibit very similar Δv values. However, the fifth case is the best candidate to have the most cost-effective mission configuration by a large margin and is subjected to three *Matlab* solver functions to find the minimum value, in increasing degree of function evaluations. The results are seen in Table 1.2.

Function	Optimum Δv [km/s]	Departure Date	Departure Time	ToF to GA [days]	ToF to NEO [days]
fminunc	16.8599	16/8/2031	13:48:45	1426.68	1558.86
patternsearch	16.8597	16/8/2031	9:56:59	1426.84	1558.91
particleswarm	16.8597	16/8/2031	7:35:36	1426.94	1558.91

Table 1.2: Comparison in Minimization Solver Solutions

All three solvers agree on the optimum result with respect to the mission cost, only deviating on the dates of each manoeuvre. Nonetheless, given the fact that this project deals with an approximation method of patched conics and ideal burn procedures, it is safe to say that the best case has been found. The optimum mission is therefore chosen as the `particleswarm` solver solution, seen in Table 1.3.

Optimum Δv [km/s]	16.8597	**GA Date**	13/7/2035 - 6:05:33
Departure Date	16/8/2031 - 7:35:36	**Arrival Date**	19/10/2039 - 3:57:06

Table 1.3: Best Mission Dates

1.4.1 Heliocentric Trajectories

The best solver solution seen in Section 1.4 is plotted in Figure 1.4. The position of Earth, Saturn and NEO at Departure, Gravity Assist and Arrival are also plotted, denoted *Dep*, *GA* and *Arr*, respectively. The Earth-Saturn Transfer has a semi-major axis of 5.5185 AU and an eccentricity of 0.8162, whereas the second transfer arc has the values 5.1130 and 0.8761 respectively.

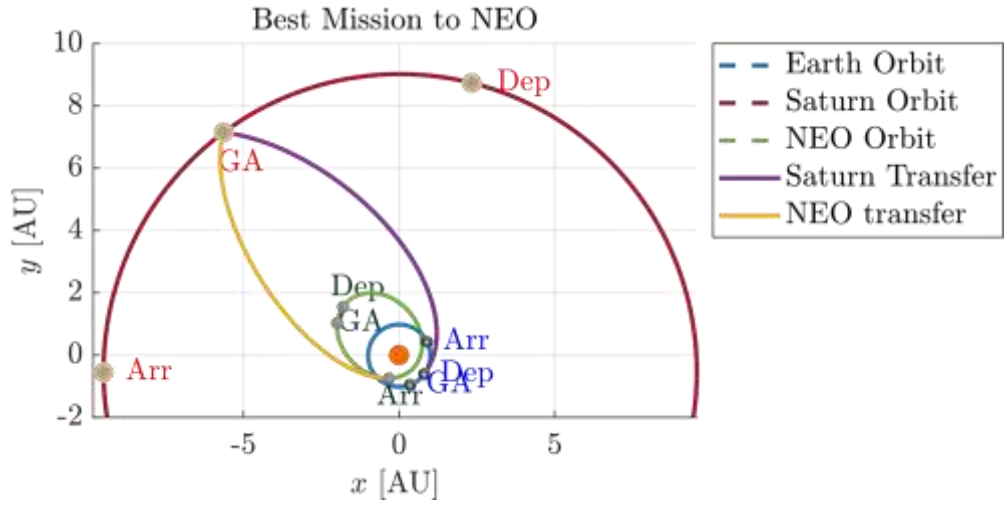

Figure 1.4: Best Mission - Heliocentric Plot

1.4.2 Powered Gravity Assist

The initial and final velocities computed from the Lambert Arc solutions combined with Saturn's velocity at Gravity Assist time are used to define the incoming and outgoing velocities of the hyperbolic trajectory. In the patch conics approximation, the SOI of Saturn is considered point-like and the time of transfer is not in this manoeuvre is not taken into account. However, this region radially extends 895 times Saturn's Radius and leads to mission duration miss-matches, as the fly-by time is over 162 days. Table 1.4 showcases the Gravity Assist Parameters, with the distance values also expressed in terms of Saturn's Radius between brackets for a more visual understanding.

R_{Saturn} **[km]**	58232	Δv **fly-by [km/s]**	7.09491	δ^{-} **[deg]**	60.1561
delta [deg]	60.1563	Δv **GA [km/s]**	1.74182E-5	δ^{+} **[deg]**	60.1564
Δ **[km] (Rs)**	1307529 (22.4538)	$a^{'}$ **[km] (Rs)**	-757281 (13.0046)	e^{-}	1.99529
R_p **[km] (Rs)**	753716 (12.9433)	$a^{`}$ **[km] (Rs)**	-757287 (13.0047)	e^{+}	1.99529

Table 1.4: Hyperbolic Trajectory - Gravity Assist Parameters

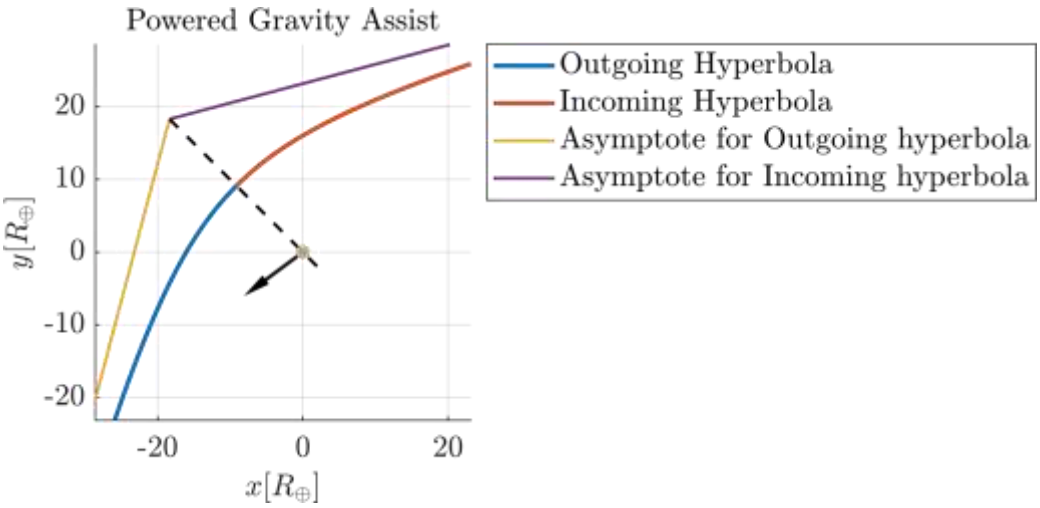

Figure 1.5: Hyperbolic Gravity Assist - Saturn Centered - Heliocentric Reference

1.5 Results and Conclusions

The three total Δv change manoeuvres are seen below. The burn performed at Gravity Assist is minute in comparison with the other burns, almost rendering this mission as a pure fly-by. It makes sense, however, given that the spacecraft effectively desires to lower its perihelion from that of the departure planet (Earth) to the NEO's perihelion as seen in Figure 1.4. As the distance of Saturn is very large, this results in a very small burn to decrease the lowest orbit point.

Furthermore, the most resource-consuming operation involves the heliocentric inclination change. Saturn is inclined 2.487º with respect to the ecliptic plane, which highly increases the cost requirements for departure. It is therefore why the optimum mission performs the second transfer arc after the gravity assist in the same 2.198º inclination as the NEO orbit. This project serves a good exercise to explore the design iteration process in designing interplanetary missions involving several DoFs. In reality, a mission like this would require several intermediate fly-by's and deep space manoeuvres to reach Saturn and the NEO to reduce the cost, with the implementation of specialized genetic algorithms to obtain a suitable solution given the increased number of DoF's.

Δv **departure [km/s]**	10.6666	Δv **arrival [km/s]**	6.19308
Δv **GA [km/s]**	1.74182E-5	Δv **Total [km/s]**	16.8597

2. *Planetary Explorer Mission*

2.1 Mission Description

The *PoliMi Space Agency* wants to launch a **Planetary Explorer Mission**, to perform Earth observation. To do this, an orbit analysis and a ground track estimation have been carried out. The perturbations considered in the model are Moon gravity disturbance force, and the first zonal harmonic J2, due to Earth's oblateness.

2.2 Nominal Orbit Characteristics

The provided initial orbit parameters, a, e and i collocate the satellite in the Medium Earth Orbit (**MEO**) region. The remaining three Keplerian elements Ω, ω and θ are left for the team to choose, so the ones of the real object that is going to be studied in section 2.7 were used, taken from [3]. The initial conditions are thus the ones shown in table 2.1. To visualize the orbit, the initial conditions are propagated solving the differential equation of the restricted two-body problem over one period.

a [km]	e [-]	i [deg]	Ω [deg]	ω [deg]	θ [deg]
15756	0.5297	30.1666	112.79	302.048	162.48414

Table 2.1: Nominal Keplerian elements

2.3 Perturbations

The introduction of a perturbing acceleration modifies the equations of motion into 2.1. The perturbing acceleration is written in Cartesian coordinate.

$$\ddot{\mathbf{r}} = -\frac{\mu_C}{r^3}\mathbf{r} + \mathbf{a}_p \tag{2.1}$$

a_p represent the disturbance acceleration from each source other than spherically symmetric gravitational attraction between two bodies. The accelerations taken into consideration are modelled as follows:

1. J2 acceleration

$$\mathbf{a}_{xyzJ2} = \frac{3}{2} J_2 \mu_C R_C^2 \left[\frac{x}{r^4} \left(5\frac{z^2}{r^2} - 1 \right) \hat{\mathbf{i}} + \frac{y}{r^4} \left(5\frac{z^2}{r^2} - 1 \right) \hat{\mathbf{j}} + \frac{z}{r^4} \left(5\frac{z^2}{r^2} - 3 \right) \hat{\mathbf{k}} \right] \quad (2.2)$$

Where:

- J2= 0.00108263 is the first zonal harmonic coefficient;
- r is the distance of the s/c from the centre of the Earth;
- μ_C and R_C are the Earth's gravitational parameter and radius respectively;

2. Moon Gravity Disturbance Force

$$\mathbf{a}_{xyzK} = \frac{3\mu_K \hat{\mathbf{r}}_{3K/SC}}{r_{K/SC}^3} - \frac{\mu_{K3} \hat{\mathbf{R}}_{3K}}{R_K^3} \quad (2.3)$$

Where:

- $\mu_K = 4.902801 \cdot 10^3$ is the gravitational parameter of the Moon; • $r_{K/SC}$ is the distance of the s/c from the centre of the Moon;
- $\hat{\mathbf{r}}_{K/SC}$ is the radial unit vector from the Moon to the spacecraft;
- R_K is the distance between Moon and Earth;
- $\hat{\mathbf{R}}_K$ is the radial unit vector of the Moon from the Earth;

Under the effect of those perturbations, the orbit evolves as shown in figure 2.1.

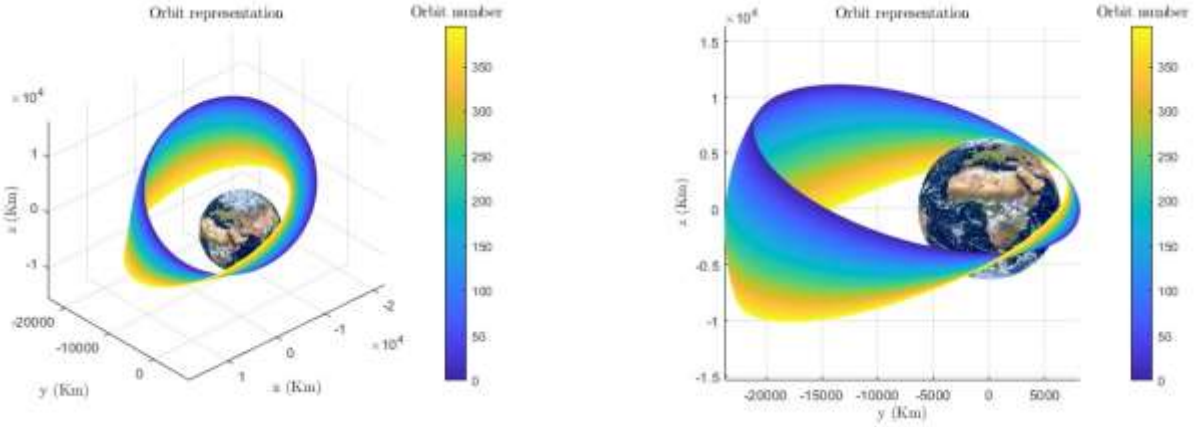

Figure 2.1: Orbit representation.

2.4 Ground Track

2.2 shows the ground tracks over different periods, with or without disturbances. Without disturbances it is observable a westward shift per orbit of the satellite on the ground track due to Earth rotation, that matches the prediction of equation 2.4. It can also be observed that the maximum latitude the ground track reached is equal to the inclination of the orbit.

$$\Delta\lambda = T\omega_E = 2\pi\frac{T}{T_E} = 82.01^\circ \quad (2.4)$$

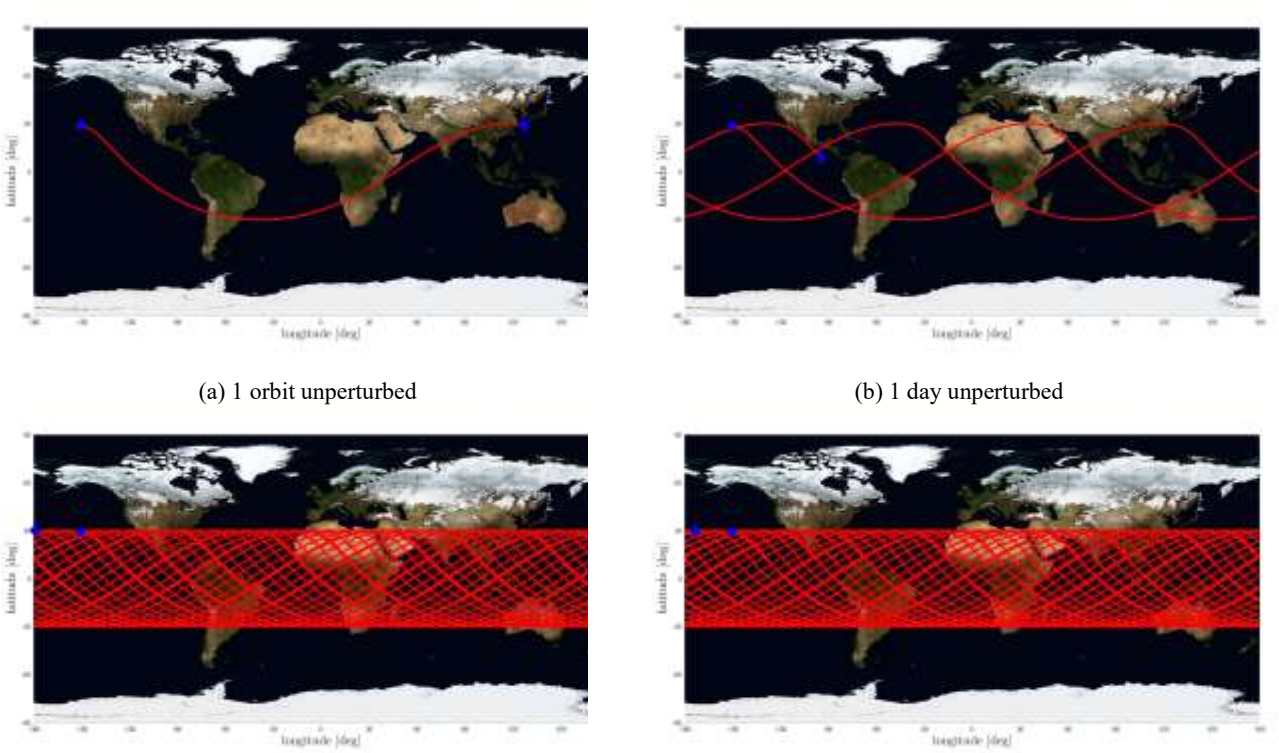

(a) 1 orbit unperturbed

(b) 1 day unperturbed

(c) 10 days unperturbed

(d) 10 days perturbed

Figure 2.2: Unperturbed and perturbed non-repeating ground track for different propagation times

2.5 Repeating Ground Tracks

To obtain a repeating ground track, the shift of the trace of the s/c in k orbits must be equal to the Earth's rotation in m sidereal days, which means imposing $k\Delta\lambda = m2\pi$. With the assigned repeating ground track ratio (i.e. 13:3), the semi-major axis of the orbit can be modified for this condition to be verified:

$$a_{rep} = n^{-2} = 15864.122Km \tag{2.5}$$

where n is the mean motion of the modified orbit, chosen such that

$$\frac{T_E}{T} = \frac{k}{m} \Longrightarrow n = \omega_E \frac{k}{m} \tag{2.6}$$

Concerning about the ground tracks for the orbit with the modified semi-major axis, in the unperturbed case the ground track repeats itself perfectly, while considering the perturbations this result is not achieved. 2.3 shows this latter aspect, for a time frame of 13 periods (i.e. number of periods needed to complete a repeated ground track).

2.6 Perturbed orbit propagation

The propagation of the orbit can be achieved either integrating the equation of the perturbed two-body problem using cartesian coordinates or working on the Keplerian Elements through the Gauss' planetary equations. The first method consists of solving the differential equation 2.1 to find the state of the satellite at each time instant in Cartesian coordinates, and then converting the cartesian state to keplerian through the *car2kep* function. The second method needs the integration of Gauss' planetary equations, from [2], in this case in the *radial-transversal-out of plane* reference frame, listed in 2.7.

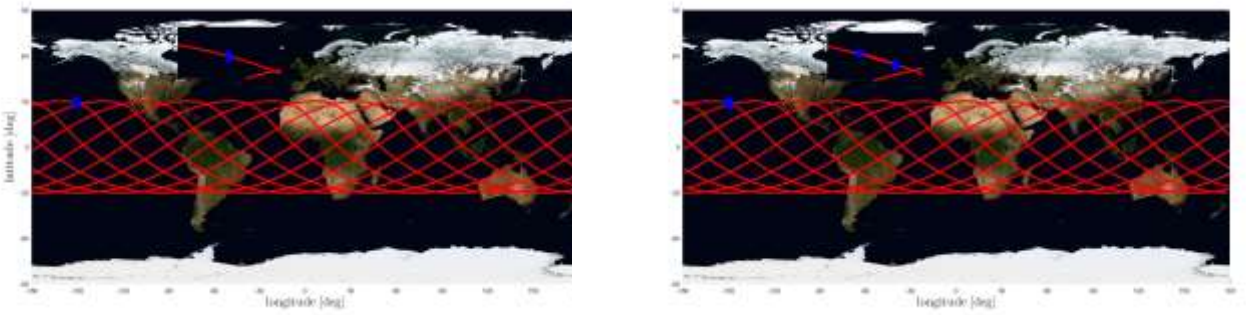

(a) 13 orbits (b) 13 orbits

Figure 2.3: Unperturbed (left) and perturbed (right) repeating ground track

$$\begin{aligned}
\frac{da}{dt} &= 2\frac{a^2}{h}\left(e\sin(\theta)a_r + \frac{p}{r}a_s\right) \\
\frac{de}{dt} &= \frac{1}{h}\left(p\sin(\theta)a_r + \left((p+r)\cos(\theta) + re\right)a_s\right) \\
\frac{di}{dt} &= \frac{r\cos(\theta+\omega)}{a_w} \\
\frac{d\Omega}{dt} &= \frac{r\sin(\theta+\omega)}{h\sin(i)}a_w \\
\frac{d\omega}{dt} &= \frac{1}{he}\left(-p\cos(\theta)a_r + (p+r)\sin(\theta)a_s\right) - \frac{r\sin(\theta+\omega)\cos(i)}{h\sin(i)}a_w \\
\frac{d\theta}{dt} &= \frac{r^2}{h} + \frac{1}{eh}\left(p\cos(\theta)a_r - (p+r)\sin(\theta)a_s\right)
\end{aligned} \tag{2.7}$$

where a_r, a_s and a_w are the components of the perturbing acceleration in the *RSW* frame (2.8), with the versors calculated as in 2.9.

$$\mathbf{a} = a_r\hat{\mathbf{r}} + a_s\hat{\mathbf{s}} + a_w\mathbf{w}\hat{} \tag{2.8}$$

$$\hat{r} = \frac{\mathbf{r}}{r} \qquad \hat{w} = \frac{\mathbf{r}\times\mathbf{v}}{\|\mathbf{r}\times\mathbf{v}\|} \qquad \hat{s} = \hat{w}\times\hat{r} \tag{2.9}$$

With both computing approaches we reach the same orbit. In figure 2.4 the relative error between both methods is calculated, and in the worst case it is in the order of 10^{-8}, so it is safe to assume that both methods are coherent. However, in table 2.2 we can see that Gauss equations are computationally faster than Cartesian integration, even without taking into account that the results of the second need to be processed to obtain the Keplerian elements.

	Gauss planetary equations	Cartesian coordinates
Elapsed time [s]	5.8	7.6

Table 2.2: CPU time of each method.

The error between the propagation in Cartesian coordinates or with Gauss equations is shown in figure 2.4. The evolution of the elements can be shown in figures 2.6 for a comparison with a real satellite and in 2.5 decomposed in the short, long and secular terms.

Finally, it is worth mentioning that figure 2.5 show a behaviour for the secular term of argument of perigee and right ascension of the ascending node that matches the theoretical values given by equations 2.10 and 2.11, taken from [B]: $3\,c\mu^{C}\hat{}\,R^{C}\cdot_2 \quad 3\,c\mu^{C}\hat{}\,R^{C}\cdot_2{}^2$

$\Omega 9 = -2J_2 \quad \overline{a_3} \quad \overline{ap1-e2q} \quad cospiq = -0.7009 deg\{day \qquad \omega 9 = -4J_2 \quad \overline{a_3} \quad \overline{ap1-e2q} \quad p5cos\,piq-1q = 1.1096 deg\{day$

(2.10) (2.11)

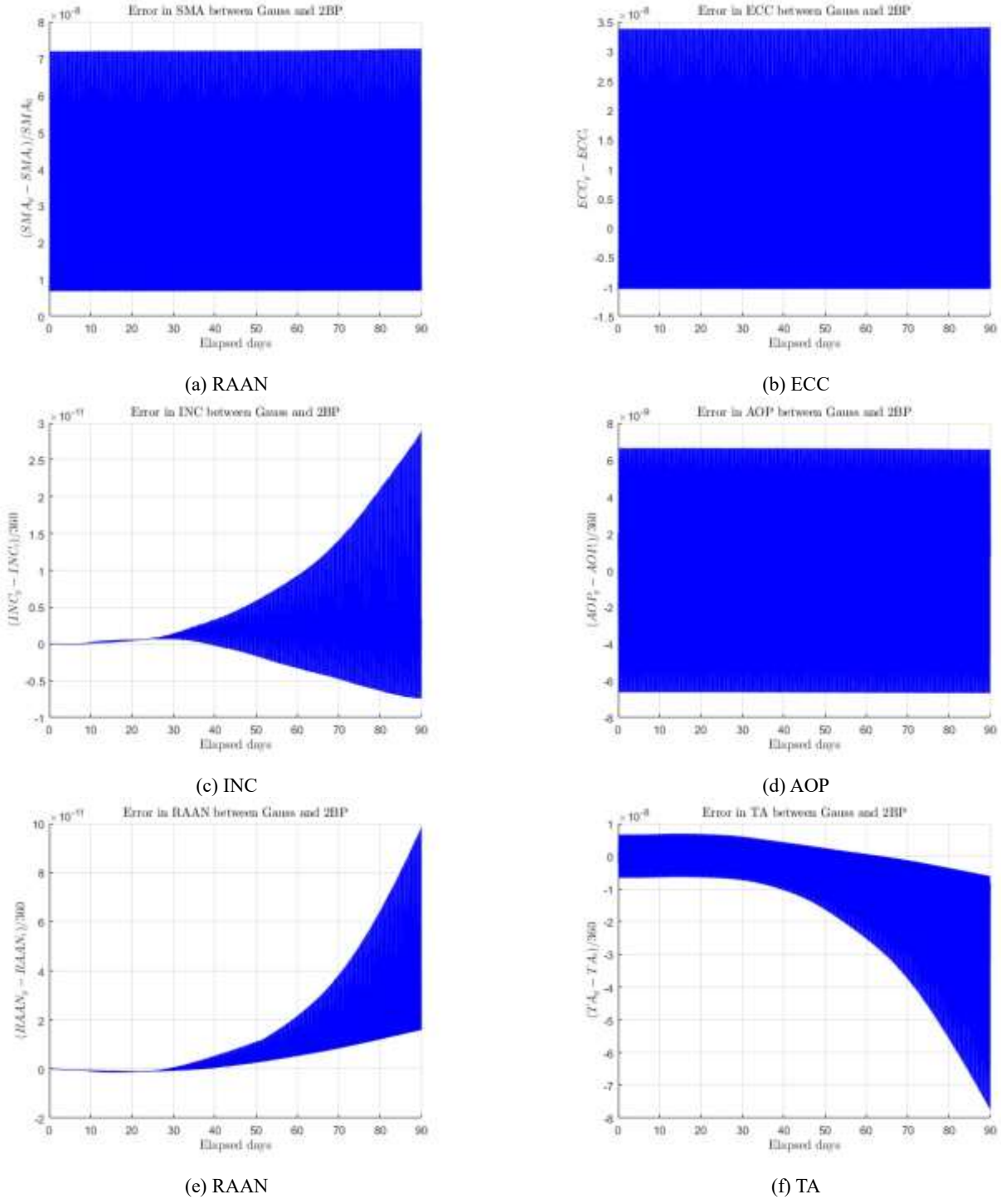

(a) RAAN (b) ECC

(c) INC (d) AOP

(e) RAAN (f) TA

Figure 2.4: Errors between each propagation method.

2.6.1 Filtering

The perturbations that we have taken into account in our simulation differs in period and so they affect the orbital elements causing oscillations with different frequencies. The MATLAB function *movemean* can be used as a low-pass filter, in order to remove the higher frequency components and keeping the slower ones, depending on the cut off frequency. For the J_2 and Moon perturbations, it has been assumed that the first has a period equal to the one of the rotation of the satellite and the second equal to the rotation of the Moon. Data shows that the perturbations caused by the Moon have in fact a period equal to half of the one of the Moon. In 2.5 is clearly visible also the Gibbs phenomenon.

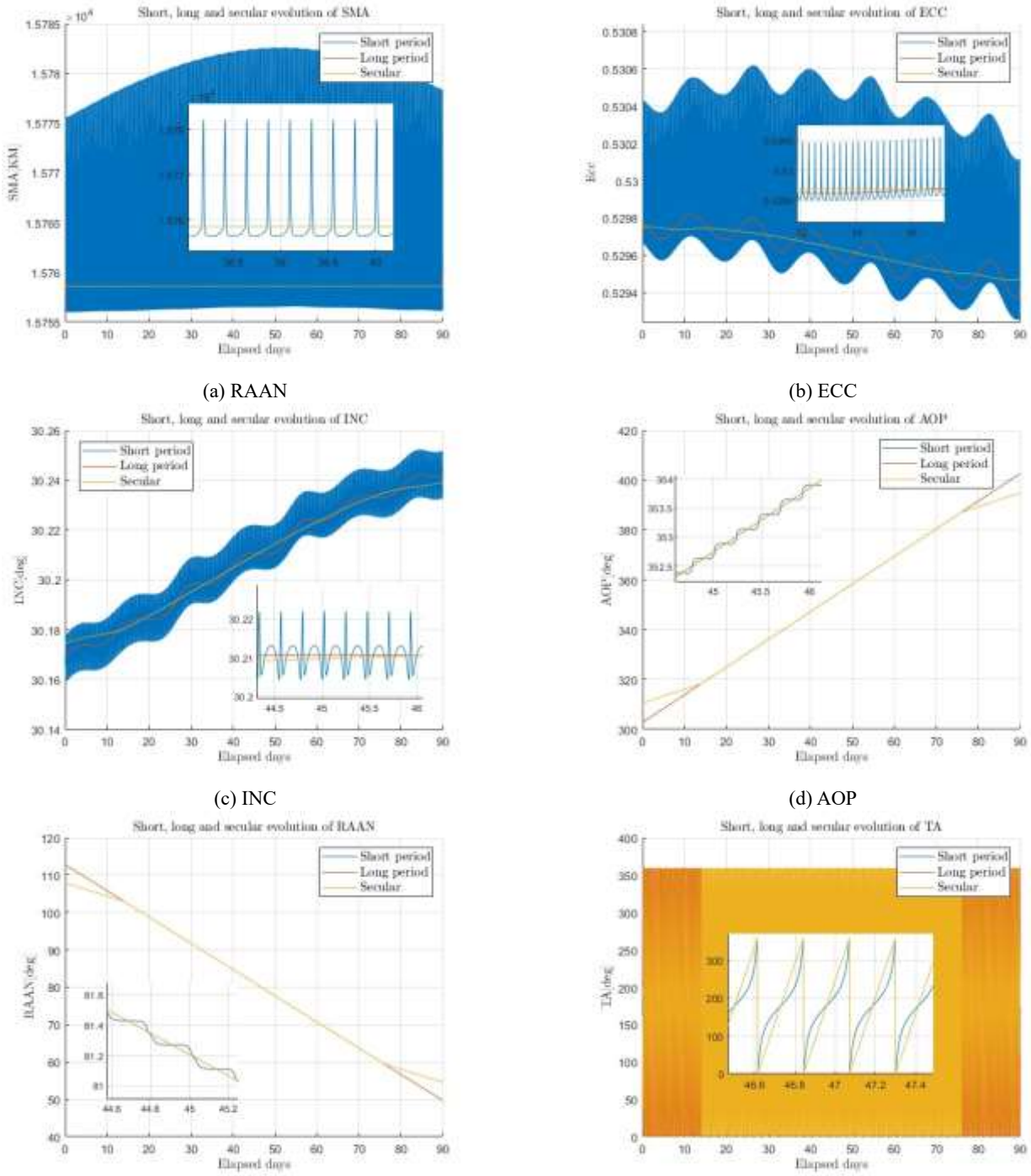

(a) RAAN (b) ECC

(c) INC (d) AOP

(e) RAAN (f) TA

Figure 2.5: Short, long and secular elements of the perturbations.

Looking at the figures that the J2 is mainly responsible for the short term perturbations and the Moon for the long term ones, while the secular component is shared between both. It can also be seen that only eccentricity and inclination are affected by long term oscillations, the other elements only have short term or secular ones.

2.7 Comparison with real data

To understand whether our model is appropriate, we compared the orbit propagate on our own with the one of a real world object. The orbiting object we selected is COMETS, present on the NORAD CAT ID as 25175, founded in the catalogue of SPACETRACK website. It's RAAN, AOP and TA are being used to set other initial conditions not specified in the assigned data.

a [km]	e [-]	i [deg]	Ω [deg]	ω [deg]	θ [deg]

15758.7167	0.5293	31.4018	302.804	112.923	162.48414

Table 2.3: Orbit elements

The evolution of the orbital elements has been downloaded from NASA Horizons and plotted, together with the evolution obtained propagating the same initial conditions with Gauss planetary equations and with Cartesian coordinates. The time span selected (3 months) was taken so it is enough for the slower disturbing effect (the Moon) to fully manifest it's effect.

Looking at the results, its clear that while some similarities with reality are captured in the model, such as the period of the short and long term disturbances or the general behaviour of AOP or RAAN, in general the evolution of real and modelled data is not the same. This is due to the fact that lots of disturbance effects have not been considered. The main ones are higher order elements of the geopotential, as the altitude of the satellite is not enough (perigee altitude is around 1000 Km) to neglect all except J2 and solar radiation pressure, which could be the responsible of the decrease of inclination that the real satellite experiments and the model does not. Finally, the atmospheric drag at 1000 Km is not a very important effect, but is also not negligible and could be relevant in a propagation longer than 90 days.

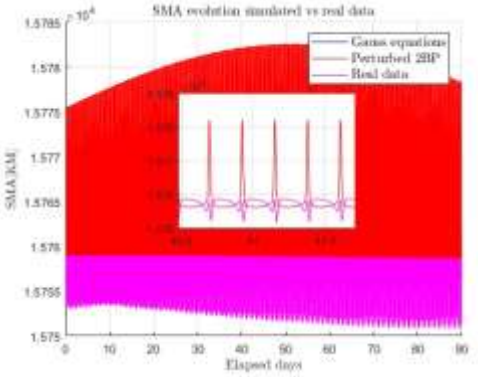

(a) RAAN

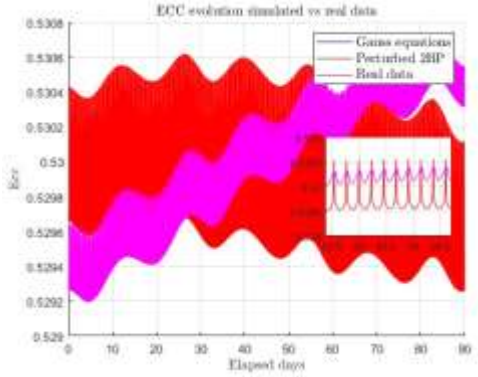

(b) ECC

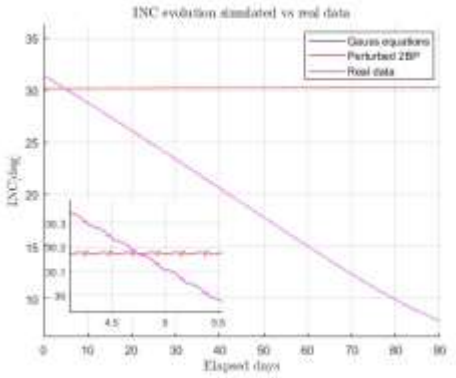

(c) INC

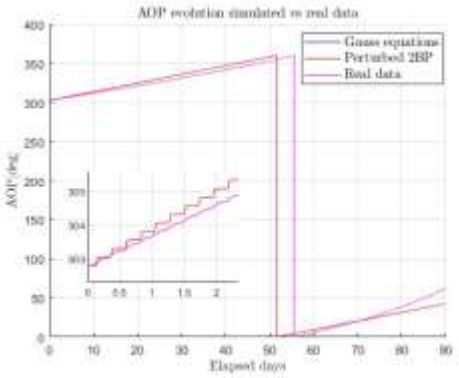

(d) AOP

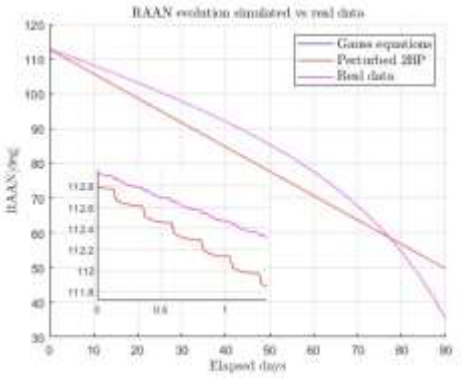

(e) RAAN

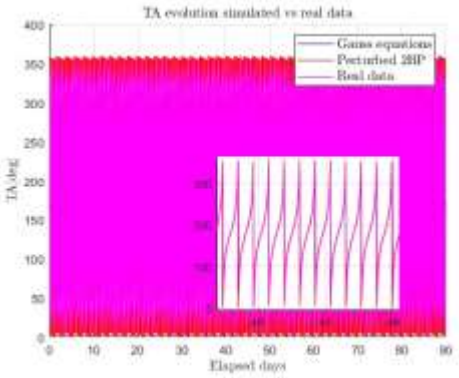

(f) TA

Figure 2.6: Errors between each propagation method.

2.8 Conclusions

From the analysis of the unperturbed and perturbed ground tracks, it can be stated that the model corresponds to a good representation of the real behaviour of the spacecraft, since the ground track:

- Crosses two times the equator for each revolution;
- Has one maximum and one minimum value for the latitude, that remains equal to the inclination;
- Presents a shift in longitude on each pass through the equator of a value that corresponds to the theoretical one, as in equation 2.4;

Regarding the repeating ground tracks, satisfying results were achieved too:

- Modifying the semi-major axis, the ground track of the unperturbed orbit repeats itself perfectly. After a whole cycle of k orbits or m days is completed, the initial and final points coincide.
- Considering the perturbations, the ground track does not repeat itself exactly, since the nodal periods $T\hat{}_E$ and $T\hat{}$ no longer correspond to T_E and T, because the orbital elements are modified by moon gravitational force and zonal harmonic;

Regarding the comparison between propagators:

- The result given by both methods are almost the same.
- Gauss equations are faster than Cartesian integration in terms of CPU time.

Regarding to the evolution of the elements:

- The long term variation of the RAAN and AOP corresponds to the theoretical one as shown in equations 2.10 and 2.11;
- They present oscillations with different periods, related to the period of the disturbing effects.
- More perturbations need to be considered to replicate the behaviour of a real object.

Bibliography

[1] NASA - June 2004 - *Cassini-Huygens* Saturn Arrival

[2] Juan Luis Gonzalo Gomez, Lorenzo Giudici, Camilla Colombo, Orbital mechanics Course Slides, MSc Space Engineering, A.Y. 2022/2023

[3] Space-Track https://www.space-track.org